Journal of Applied Fluid Mechanics, Vol. 18, No. 1, pp. 112-130, 2025.
Available online at www.jafmonline.net, ISSN 1735-3572, EISSN 1735-3645.
https://doi.org/10.47176/jafm.18.1.2886

Airwake Characteristics of NATO-Generic Destroyer: A Numerical Study

S. Sari[1†], A. Dogrul[2] and S. Bayraktar[3]

[1] *Yildiz Technical University, Department of Naval Architecture and Marine Engineering, 34349 Istanbul, Turkiye*
[2] *National Defense University, Turkish Naval Academy, Department of Naval Architecture and Marine Engineering, 34942 Istanbul, Turkiye*
[3] *Yildiz Technical University, Department of Marine Engineering, 34349 Istanbul, Turkiye*

†*Corresponding Author Email: sarih@yildiz.edu.tr*

ABSTRACT

This paper presents a numerical investigation of the air wake around a generic surface combatant ship called NATO-Generic Destroyer (NATO-GD). Naval surface combatants with flight decks must be designed taking aerodynamic concerns into account. Most of the previous studies have employed the Simple Frigate Shape (SFS) and its modified version (SFS2) to investigate the airwake. However, these generic geometries do not accurately represent modern warship designs. To address this, a modern geometry called NATO-GD proposed by the NATO Research Task Group, which represents the features of a modern destroyer, was utilized in the present work. The objective is to examine the air wake on the helicopter deck to ensure the safe operation of air vehicles such as helicopters and drones. The three-dimensional, transient airflow around the ship was solved using the unsteady Reynolds-Averaged Navier-Stokes (URANS) and Detached Eddy Simulation (DES) turbulence models. Besides, the effect of inflow was investigated by comparing uniform velocity inlet and atmospheric boundary layer (ABL) for various wind-over-deck (WOD) angles. The numerical approach was verified for the URANS turbulence model using the Grid Convergence Index (GCI) method. The numerical uncertainty was calculated with four different methods and the uncertainty was found between 1.6% and 2.1%. A detailed discussion of the flow field above the flight deck was conducted to compare the URANS and DES models fairly. It was concluded that employing the ABL profile as a boundary condition is more suitable for achieving accurate ship aerodynamics calculations. The ABL velocity profile makes a significant difference in the velocity components. According to the URANS results, these deviations are found as 8.23% in the x-component, 1.25% in the y-component and 4.89% in the z-component. The deviations were calculated using the root mean square error (RMSE) method. Furthermore, although the numerical results of the URANS and DES models were similar at some points, detailed flow field analysis is only possible with the DES results to determine safe approach patterns for air vehicles. Various wind speeds, directions, and the resulting wake structures were tested to analyze the wake behavior over the helicopter deck under different air conditions. When the wind comes from the port side with 15 degrees (R15) it wind changes the intense turbulence region and creates a low turbulence area on the starboard side while R30 wind causes small scale vortices breaking this region.

Article History

Received May 30, 2024
Revised July 30, 2024
Accepted August 26, 2024
Available online November 6, 2024

Keywords:

DES
GCI
NATO-GD
Ship Airwake
Turbulence
URANS

1. INTRODUCTION

Although ship design generally focuses on hydrodynamic and structural problems, aerodynamic effects on the ship's superstructure should also be considered because the interaction between the air and the superstructure affects the safety of the crew and the aircraft, specifically when the ship is equipped with a flight deck. In addition, wind loads acting on the ship's hull should be determined for various wind-over-deck (WOD)

Nomenclature

ρ	density
U_i	velocity vector
P	pressure
υ	kinematic viscosity
Δ_{max}	maximum edge length of the local grid
k	turbulent kinetic energy
ω	specific dissipation rate
K	Von Karman constant
z_0	aerodynamic roughness
z_{ref}	reference height
u_{ref}	reference velocity
R	convergence condition
$\emptyset_i$	scalar function
U_N	numerical uncertainty

Abbreviation List

ABL	Atmospheric Boundary Layer
CFD	Computational Fluid Dynamics
DES	Detached Eddy Simulation
GCI	Grid Convergence Index
IDDES	Improved Delayed Detached Eddy Simulation
LES	Large Eddy Simulation
NATO	North Atlantic Treaty Organization
NATO-GD	NATO-Generic Destroyer
ONRT	Office of Naval Research Tumblehome
PIV	Particle Image Velocimetry
PSD	Power Spectral Density
RMSE	Root Mean Square Error
SFS	Simple Frigate Ship
SHOL	Safe Helicopter Operation Limits
SST	Shear Stress Transport
URANS	Unsteady Reynolds-Averaged Navier-Stokes
WOD	Wind Over Deck

angles, which have significant impacts on the ship's stability and maneuvering. In this manner, naval surface platforms, specifically equipped with a flight deck, come into mind firstly because these platforms are designed for high expectations in terms of operability, mobility and survivability. In these aspects, the superstructure needs to be designed with aerodynamics in mind. So, not only the geometrical design but also the arrangement and integration of the systems located on the superstructure can be optimized. The most crucial phenomenon to consider is safe helicopter operations because, ~~both~~ the helicopter, ship and their crew may be in significant danger in this case.

The aerodynamics of floating bodies can be studied by experimental and/or numerical methods. Traditionally, the experiments are carried out at different WOD angles and wind speeds in model scale using wind tunnels. On the other hand, the numerical studies are performed using in-house or commercial computational fluid dynamics (CFD) solvers. As a strong numerical technique, the CFD method enables the interpretation of the flow field in detail. Within this perspective, several studies have been made focusing on the ship airwake using benchmark ship geometries. Mostly, SFS and SFS2 models were preferred in the related literature (Reddy et al., 2000; Setiawan et al., 2022; Zhu et al., 2022). Forrest and Owen, (2010) focused on the airwake of the SFS2 and Royal Navy Type 23 frigate. They compared the experimental data with DES results and modeled the turbulence effects. A validation study was conducted by Yuan et al. (2018) using SFS2 ship geometry. Upon successful validation, a Canadian patrol frigate was inspected with the Delayed DES model. The effect of the mast geometry was examined and a good agreement was achieved with the experiments. Using experimental and numerical techniques low-velocity recirculation areas above the flight deck were studied by Bardera et al. (2019). The purpose of the study was to examine the effects of helicopter rotor on the SFS2 generic ship regarding helicopter operational limits. As a result, the effect of the helicopter rotor on complex maneuvers at different turbulence intensities was determined. In another study, the authors conducted numerical analyses and paid special attention to the optimum length of hangar employing SFS and SFS2 generic ships. Even the small eddies were captured using the DDES model (Li et al., 2020). Gnanamanickam et al. (2020) used the PIV technique by employing ABL for airwake over a 1/90 scale modeled SFS2 generic ship. By conducting several measurements of the airwake at five longitudinal (streamwise) planes, they managed to identify three regions of recirculating flows over the rear of the ship, including the flight deck that is subjected to large-scale correlated motions. Nisham et al. (2021) utilized the DES turbulence model in full-scale SFS2 analyses considering the wave conditions with different WOD angles and wave frequencies. They reported the effects of the atmospheric boundary layer (ABL). Taymourtash et al. (2022) conducted wind tunnel tests on a scaled helicopter near a generic frigate model to measure unsteady aerodynamic loads. The tests involved simulating a stern landing maneuver, and the rotor parameters were obtained. The study identified both average loads and frequency spectrum relevant to flight performance. The results show that the unsteadiness of the loads increases when moving toward the landing spot for various wind directions. Using a high-speed stereoscopic PIV in a low-speed wind tunnel (WT) Zhu et al. (2023) compared the airwake development over a 1/90 SFS2 model with and without ABL. They reported diffused airwake and intense horseshoe vortex around the funnel when ABL was used. In a recent study, Major et al. (2023) studied time-varying full-scale ABL on the characteristics of the SFS2 ship airwake for various WOD ranging from headwind (WOD=0 degree) to 60 degrees with a 15-degree increment. It was concluded that the atmospheric boundary layer of different levels has little effect on the velocity profile at WOD=0 degree, however, at WOD=-60 degrees interaction of the turbulent eddies with the vortex structures of airwake over the flight deck is significant. However, these geometries are very simple as they are called simple frigate ships (not having an underwater form) and the purpose of using these geometries is to pay attention to the importance of ship airwake phenomenon by providing experimental data to the literature.

Therefore, a newly proposed naval surface combatant, namely ONRT, was used in some studies by conducting PIV experiments in a water tunnel (Dooley et al., 2020a). In another study, Dooley et al. (2020b) used an in-house CFD code REX for the effects of wind, regular head waves and ship motions on airwake and helicopter operating above the flight deck of ONRT. A generic helicopter model based on Sikorsky SH-60 Seahawk was used for simulations. They considered several cases such as the ship only, the ship and helicopter and helicopter only, specifically when the helicopter is operating under the influence of the motions of the ship and waves.

Apart from these benchmark geometries, some studies have focused on existing naval platforms to simulate the ship airwake and/or ship-helicopter interaction. Bogstad et al. (2002) investigated the ship airwake of five different Royal Navy ships using the Reynolds-Averaged Navier-Stokes (RANS) method. They validated their numerical data with the experimental results of a Canadian patrol frigate. The analyses were then extended to various wind directions and speeds. The main purpose was to create a database for the flight simulator of the Merlin-class helicopter. The other experimental research in the model scale of an aircraft carrier submerged in a circulation channel was shown in the study of Watson et al. (2019). The unsteady flow around the superstructure of the ship was measured using Acoustic Doppler Velocimetry. In addition to outlining CFD comparisons with compact methodology descriptions, the study examined scaling concerns and covered the experimental methods. Su et al. (2019) performed simulations of a navy helicopter during vertical landing and analyzed rotor loads and pilot workload. Results show the need to adjust control inputs for rotor stabilization. Rotor aerodynamics can couple and increase unsteady loadings. The hangar bay kept open reduces pilot workload, and a closer landing spot decreases load levels. Shi et al. (2020) examined the ship-helo interaction for the landing of two helicopters on a Landing Platform Dock (LPD) and frigate numerically. Different positions of the helicopters were compared within the aerodynamic effects. For this purpose, the effect of different heights and wind-over-deck (WOD) angles on the landing performance was investigated. The turbulent fluctuations obtained from an LES simulation were incorporated into the ABL for flow over a generic landing platform dock (LPD) by Shipman and Bin (2021) and the flow field was compared with the steady inflow profile. It is seen that the complex flow field cannot be obtained when a steady uniform inflow condition is used.

Finally, the most complex ship geometry having a realistic superstructure and underwater form was proposed by the NATO Research Task Group, namely NATO Generic Destroyer (NATO-GD), in which a comprehensive experimental data set was also provided for calm water and regular wave scenarios. Unlike the studies for SFS and SFS2, the studies on the NATO-GD model are quite rare in the related literature. Owen et al. (2021) examined the relationship between a helicopter and a ship, where a pilot must maneuver the aircraft on the landing deck while navigating a moving deck and ship airwake. In their research, the airwake is modeled by CFD and wind tunnel tests, frequently employing the Simple Frigate Shape (SFS), a general ship geometry. In addition to reviewing SFS contributions, the paper presents an original vessel geometry intended for subsequent research: the NATO-GD, which represents contemporary combat ships equipped with helicopters. To promote research on how ship motion affects the airwake, it also introduces ship motion profiles. In a recent study, Setiawan et al. compared the effects of inflow conditions such as uniform inflow and ABL on SFS2 and NATO-GD. The experimental studies revealed that ABL distinctly affects the flow fluctuations while improving the wake length. They reported that ABL improves the turbulence kinetic energy on the flight deck when NATO-GD is used instead of SFS2 model geometry due to the taller geometry of the former one (Setiawan et al., 2022). In another study, the authors focused on the experimental investigation of ship airwake around Canadian patrol frigate (CPF) and NATO-GD models. Full-scale measurements were obtained for CPF and the results were compared with others in terms of power spectral density (PSD).

The literature survey indicates that several benchmark ship models were preferred for both experimental and numerical studies. However, most of the studies focused on old-fashioned models such as SFS and SFS2 which are a combination of geometric shapes while ONRT and NATO-GD ships were used in recent experimental studies. To the best of the authors' knowledge, there is not a comprehensive study including a verification study on this new generic ship form. The numerical and experimental studies lack uncertainty calculations. In addition, most of the studies focused on using DES/LES models to model the flow field and no comparison of URANS and DES/LES models has been found in the open literature. It is clear that the comparison of the numerical techniques and a detailed flow field study using the most realistic navy surface combatant model (NATO-GD), are required. In recent studies focusing on NATO-GD, only power spectral density and velocity fields were obtained.

In the present study, NATO-GD ship geometry was investigated numerically by mimicking the airflow around its superstructure and flight deck. The numerical analyses were conducted using two different turbulence models based on SST k-ω. URANS turbulence model was verified using the GCI method. The numerical uncertainty was calculated with four different methods and the uncertainty was found between 1.6% and 2.1%. After, both turbulence model results were compared with the available experimental data in terms of non-dimensional velocity components. During the analyses, Strouhal dynamic similarity was satisfied as dictated in a similar study (Owen et al., 2021) to maintain the same wind velocity with the experiments. The uniform velocity and ABL velocity profiles were defined to show the effects of ABL. According to the URANS results, these deviations are found as 8.23% in the x-component, 1.25% in the y-component and 4.89% in the z-component. The deviations were calculated using the root mean square error method. Following this, the DES turbulence model was initiated with the same ABL profile. The URANS and DES turbulence models were compared concerning flow field characteristics such as velocity, helicity in vortex cores

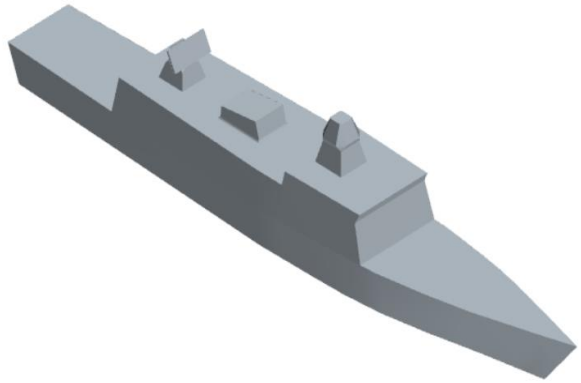

Fig. 1 3-D model of NATO-GD

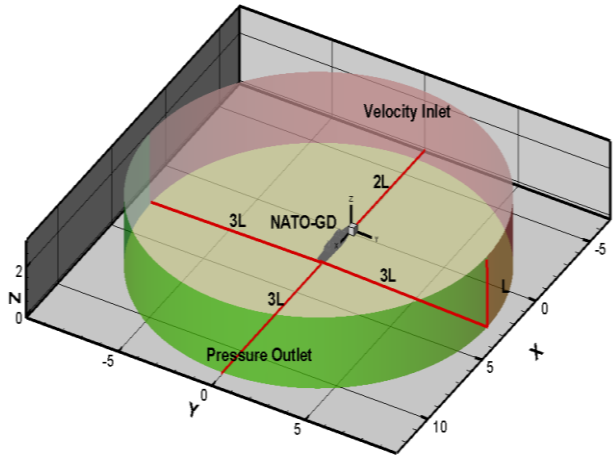

Fig. 2 Computational domain in meters and the boundary conditions

and wall shear stress. Finally, different wind angles were investigated for both turbulence models to show the effects of WOD angle on the ship's airwake. In conclusion, the URANS model gives misleading results in terms of vortex structures at various elevations over the flight deck for different WOD angles. However, the DES model shows the details of the vortices at these elevations and this would ensure the correct pattern for safe helicopter operations. Within the DES model, turbulence intensity and velocity distributions were obtained and large and small scaled vortices were captured at different elevations over the flight deck. Thus, possible approach patterns reveal for safe helicopter operations.

2. COMPUTATIONAL DETAILS

2.1 Model Geometry and Computational Domain

As aforementioned, the NATO-GD is a conceptual warship model that has a more realistic shape with respect to SFS and SFS2 geometries since it contains not only the hull section but also the mast, radar and exhaust funnel that are found on most modern warships. Although the overall length, height and breadth of the ship aft are 150 m, 30.3 m and 16.8 m, the numerical analyses were conducted with a model scale of 1/50. The main dimensions of the full-scale ship can be found in Owen et al. (2021). Figure 1 shows the 3-D model of NATO-GD from a perspective view.

Numerical studies related to the subject primarily utilize commercial and open-source softwares. For this purpose, the ship superstructure was modeled only in the air environment, mimicking the wind tunnel experiments, to examine the parameters affecting the flow around the ship. CFD simulations performed here were conducted using the finite volume method that needs high-quality small volumes called grid. Before the generation of the grid elements, the geometry was placed in a cylindrical domain as recommended by Thornhill et al. (2020). The upstream surface and the top surfaces were defined as velocity inlet while the downstream surface was dictated to be pressure outlet. The bottom surface and hull surface were defined as no-slip wall as shown in Fig. 2. Here, L is the ship overall length and the dimensions are given in meters.

While the NATO-GD generic destroyer may be symmetric about the centerline, the flow structure around/above it will not be symmetric at different wind angles. For this reason, the half-body approach was not used, instead, the full ship was represented inside a circular domain.

2.2 Mesh Structure and Physical Modeling

Numerical simulations were performed using a commercial CFD solver Siemens PLM Star CCM+ with the URANS simulation with SST-k-ω and SST k-ω based DES models solved with the finite volume method. The NATO-GD model placed into a computational domain, resembling wind tunnel conditions, neglected the free surface effects. A trimmer mesh algorithm was employed to discretize the domain with finite hexahedral volume elements. Local mesh refinements were implemented around the ship superstructure and flight deck. To accurately model the boundary layer flow, prism layers were incorporated. The wall y^+ values on the hull surface were kept below 30 and all wall y^+ approach was utilized as the wall function as included in the turbulence models. With the local mesh refinements, local y^+ values were kept below 1 on the flight deck. Figure 3 shows the global mesh structure applied on the computational domain while Fig. 4 shows the detail on the local mesh refinements around the hull and the flight deck.

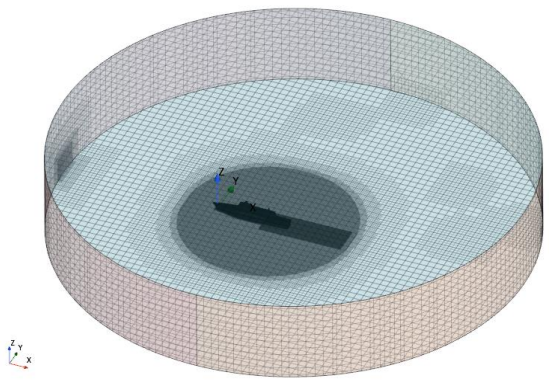

Fig. 3 Mesh structure

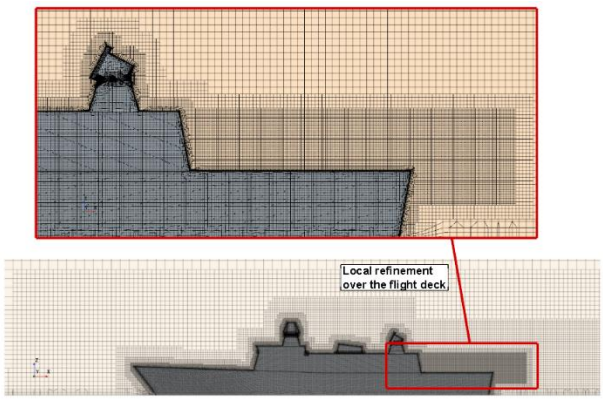

Fig. 4 Local mesh refinements

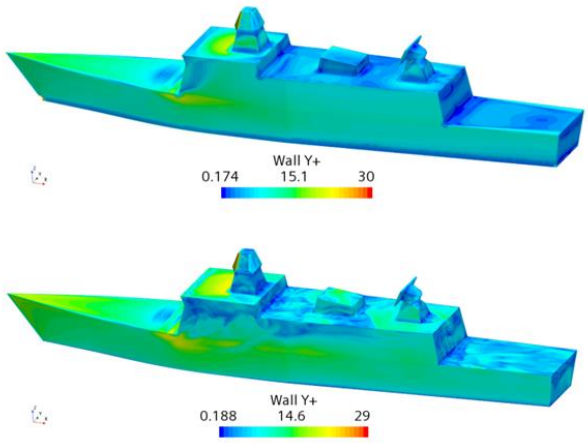

Fig. 5 Wall y^+ distribution for URANS (top) and DES (bottom)

Especially, in the DES turbulence model, local refinements were utilized with denser mesh structure to well-capture the vortex structures on the flight deck. The total cell count for URANS mesh is about 5.6 million while the total cell count for DES is about 28.9 million.

Finally, the wall y^+ distributions were given in Fig. 5 from the perspective view for both turbulence models. With the help of local refinements, y^+ values decrease on the flight deck surface.

Numerical analyses were conducted using two methods: unsteady RANS and DES turbulence models. The first approach was employed in an unsteady manner solving RANS equations. 4000 time steps were solved satisfying both numerical and scalar convergence conditions and the last 2000 time steps were used for data post-processing. DES approach was employed with a denser mesh structure for detailed flow visualization and vortex identification. In this approach, firstly 1000 iterations were run as steady RANS, following this convergence step, 4000 time steps were solved with the DES model. This approach was used in similar studies for better convergence and numerical stability (Forrest & Owen, 2010; Scott et al., 2014). In both turbulence models, the time step size was taken as 0.005 seconds. SIMPLE algorithm was employed for pressure-velocity coupling.

2.3 Governing Equations

The unsteady and fully turbulent flow over the flight deck of the NATO-GD generic ship was investigated numerically by utilizing both unsteady RANS and DES turbulence models solving the related governing equations. DES turbulence model was also utilized because the URANS approach may not simulate the highly unsteady and turbulent flow precisely when it is aimed to visualize the vortex structure in a desired region. However, the DES approach requires much higher computational resources. In the present study, both unsteady RANS (SST k-ω) and DES models were employed and their performance for air-wake over the NATO-GD were compared. The mathematical details of the models can be found in the subsequent sections.

The continuity (Eq.1) and momentum (Eq.2) equations are the governing equations for incompressible, Newtonian, isothermal and turbulent flow.

$$\frac{\partial U_i}{\partial x_i} = 0 \tag{1}$$

$$\frac{\partial U_i}{\partial t} + U_j \frac{\partial U_i}{\partial x_j} = -\frac{1}{\rho}\frac{\partial P}{\partial x_i} + \frac{\partial}{\partial x_j}\left[\upsilon\left(\frac{\partial U_i}{\partial x_j} + \frac{\partial U_j}{\partial x_i}\right)\right] - \frac{\partial \overline{u_i' u_j'}}{\partial x_j} \tag{2}$$

Here, ρ is the density, U_i states the velocity vector, and P stands for the pressure. The last two terms belong to the viscous stress tensor while υ is the kinematic viscosity.

2.3.1 SST k- ω Model

Some recent papers (Watson et al., 2019; Owen et al., 2021; Zamiri & Chung, 2023) focused on ship airwake using URANS with SST k-ω and DES turbulence models to simulate the highly complex turbulent flow over the ship's flight deck. Hence, the SST k-ω based turbulence models were employed in the present study. Detailed information about the SST k-ω turbulence model can be found in (Wilcox, 2006, 2008). The governing equations of the SST k- ω turbulence model are presented below.

$$\frac{\partial k}{\partial t} + U_j \frac{\partial k}{\partial x_j} = \frac{\partial}{\partial x_j}\left[\left(\upsilon + \sigma^* \frac{k}{\omega}\right)\frac{\partial k}{\partial x_j}\right] + P_k - \beta^* k\omega \tag{3}$$

$$\frac{\partial \omega}{\partial t} + U_j \frac{\partial k}{\partial x_j} = \frac{\partial}{\partial x_j}\left[\left(\upsilon + \sigma \frac{k}{\omega}\right)\frac{\partial \omega}{\partial x_j}\right] + \alpha \frac{\omega}{k} P_k + \beta\omega^2 + \frac{\sigma_d}{\omega}\frac{\partial k}{\partial x_j}\frac{\partial \omega}{\partial x_j} \tag{4}$$

2.3.2 Detached Eddy Simulation (DES) Model

The flow over the flight deck is separated and turbulent which makes DES suitable as reported in the literature (Yuan et al., 2016). DES method requires an additional function to switch the domain between RANS and LES. Several functions are available for this purpose. Among them, the shear stress-transport (SST) k-ω RANS model modifies diffusion term in the turbulent kinetic energy equation (Ren et al., 2022). The DES model was initially introduced by Spalart (2001) to overcome the primary limitations of LES models. It proposed a hybrid LES-RANS approach, and the blending framework served as the basis for this hybrid model. The blending framework involves a typical form where φ represents the quantity to be modeled in the momentum equation, and f is the blending factor. This hybrid model utilizes both one

equation and two equation RANS-based models. In the case of the two-equation framework, the SST k-ω model is employed. The DES formulation fully encompasses the wall boundary layers using the SST k-ω RANS model, while the free shear flows away from the walls are typically treated in LES mode. A significant advantage of the DES framework is its simplicity and its compatibility with various RANS-based models. Notably, DES is the pioneering hybrid model that allows a seamless transition between LES and URANS. For this transition having low y^+ values, the IDDES model was employed.

$$\phi^{hybrid} = f\phi^{RANS} + (1-f)\phi^{LES} \quad \text{with } 0 \le f \le 1 \tag{5}$$

$$C_{DES}\Delta_{\max} > L_t, \text{ for RANS, } C_{DES}\Delta_{\max} \le L_t, \text{ for LES, } \Delta_{\max} = \max\left(\Delta_x, \Delta_y, \Delta_z\right) \tag{6}$$

where Δ_{max} is the maximum edge length of the local grid. The two-equation model (SST k-ω) is presented as follows;

$$\frac{\partial(\rho k)}{\partial t} + \frac{\partial\left(\rho U_j k\right)}{\partial x_j} = P_k - \rho\frac{k^{3/2}}{\min\left(L_t, C_{DES}\Delta_{\max}\right)} + \frac{\partial}{\partial x_j}\left[\mu\left(\upsilon + \frac{\mu_t}{\sigma_k}\right)\frac{\partial k}{\partial x_j}\right] \tag{7}$$

$$L_t = \frac{k^{3/2}}{\varepsilon} = \frac{\sqrt{k}}{\beta^*\omega} \tag{8}$$

Detailed information about the DES turbulence model and the hybrid approach (steady RANS and unsteady DES) is available in the study of Shukla et al. (2021). More theoretical information about IDDES and DDES models can be found in Gritskevich et al. (2012).

2.4 Physics of ABL

The atmospheric boundary layer (ABL) is the lower part of the atmosphere and is affected by atmospheric processes. For a precise prediction with numerical studies, for the wind loads on high-rise buildings, bridges, wind turbines, and ground, air and sea vehicles, it is imperative to describe ABL in the CFD studies because the friction between the ground and the atmosphere is taken into account in ABL. Hence, it is important to understand flow characteristics within the ABL to consider its influences on the flow. The effect of wind conditions in ABL increases the difficulties of the flight conditions, maneuver and workload on the pilot. Numerical analyses and wind tunnel tests are conducted with an inflow directed to the ship model, however, the inflow velocity is usually considered to be uniform. This causes important negligence because the flow in nature has a velocity profile satisfying the ABL. For this reason, in some wind tunnels, fractal grids or similar structures are used to create a more realistic inflow velocity profile. In this aspect, the ABL profile can be considered also in numerical studies. For numerical studies, the importance of mesh resolution, computational domain and ABL profile were mentioned (Blocken et al., 2007).

In this study, the impacts of the ABL on the aerodynamics of the ship deck were investigated using an ABL and the power law profile (Gritskevich et al., 2012). Simulations performed with two profiles give very similar velocity distributions as shown in Fig. 6. It should be noted that not only the velocity profile but also the k (Eq. 9) and ω (Eq. 10) values were separately calculated in each

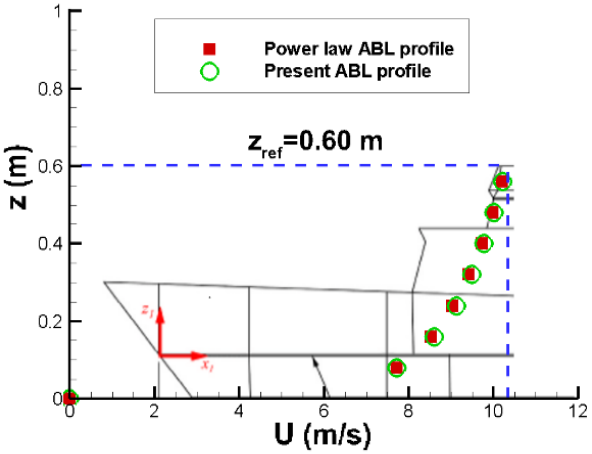

Fig. 6 Demonstration of the reference parameters and ABL profile defined in this study

position in z-direction using the below equations, instead of using default values for the ABL effects.

$$k(z) = \frac{\left(u^*\right)^2}{\sqrt{C_\mu}} \tag{9}$$

$$\omega(z) = \frac{u^*}{K\cdot\sqrt{C_\mu}}\cdot\frac{1}{z+z_0} \tag{10}$$

Here, k is the turbulent kinetic energy, ω is the specific dissipation rate. z is the height in which the velocity is calculated, K is the von Karman constant which is taken as 0.40 and z_0 is the aerodynamic roughness length which is taken as 0.0002 to represent the free surface as described (Cook, 1997; Richards & Hoxey, 1993). c_μ is turbulent viscosity constant and it is equal to 0.09 as indicated in the related reference (Cindori et al., 2022). u^* is the friction velocity and it is calculated as below.

$$u^* = K\cdot\frac{u_{ref}}{\ln\left(\frac{z_{ref}+z_0}{z_0}\right)} \tag{11}$$

where z_{ref} is the reference height as 0.60 m and u_{ref} is the reference velocity as 10.3 m/s. Figure 6 shows the reference parameters in the velocity profile. The reference height is also shown in Fig. 6 as the highest point on the ship mast where the wind anemometer is considered. In addition, the velocity profile, $u(z)$, defined in the numerical analyses is given in Fig. 6 which is calculated with the below equation.

$$u(z) = \frac{u^*}{K}\cdot\ln\left(\frac{z+z_0}{z_0}\right) \tag{12}$$

The power law velocity profile can be calculated with the following equation. Figure 6 illustrates that the ABL profile utilized in the present study matches the profile of the power law approximation.

$$u(z) = u_{ref}\cdot\left(\frac{z}{z_{ref}}\right)^{1/7} \tag{13}$$

2.5 Similarity Theory

Ship airwake studies require two scaling parameters, Reynolds (Re=UL/ν) and Strouhal (St=fL/U) numbers, to ensure kinematic and dynamic similarity. However, matching both Re and St numbers in laboratory experiments is challenging. Previous researches (Rosenfeld et al., 2015; Seth et al., 2020; Sarı et al., 2022) indicate that the flow field over the flight deck becomes independent of the Reynolds number in terms of velocity profile therefore, the similarity can be ensured for Strouhal number only.

The Strouhal number enables dynamic similarity for scaling the frequency measured in model scale to full scale. The similarity rule for the ship air-wake, based on dynamic similitude, is expressed as;

$$\left(\frac{f_s}{f_m}\right)\cdot\left(\frac{L_s}{L_m}\right)\cdot\left(\frac{U_m}{U_s}\right)=1 \tag{14}$$

Equation 14 states that the Strouhal number of the model and full-scale ship is equal so that the dynamic similarity is satisfied in terms of the Strouhal number. Here, the geometrical similarity is maintained with a scale factor of 1/50 (L_m/L_s) and the kinematic similarity is obtained with a scale factor of 1/2 (U_m/U_s). Hence, the scale factor for the frequency is 1/25 (f_m/f_s) between model and full-scale ship. The scale factors of these parameters are valid for both experimental and numerical approaches. The main reason for satisfying Strouhal similarity instead of Reynolds and Froude similarity is that the experimental results were conducted satisfying the Strouhal dynamic similarity. Reynolds similarity is difficult to maintain in the experiments because of high flow velocity, on the other hand, Froude similarity is unnecessary in the wind tunnel conditions since the experiments and analyses were carried out in single-phase (air).

3. Results and Discussion

The obtained numerical results were given in detail and compared in terms of various parameters: the existence of atmospheric boundary layer (ABL), wind over deck (WOD) angles and SST k-omega and Detached Eddy Simulation (DES) turbulence models. Firstly, the results of the unsteady RANS turbulence model were given with and without the ABL velocity profile. URANS approach was first verified using various uncertainty assessments. These results were used for the comparison of the URANS approach with the experimental data. The experimental results were presented in the open literature (Owen et al., 2021). Detailed information about the experimental setup in the wind tunnel and testing devices, and their arrangement on the ship model were given in the related references (Thornhill et al., 2020; Wall et al., 2022). Following this, DES turbulence model results were compared with the experimental data obtained from the open literature. Thus, the impacts of ABL and different turbulence models were compared. The comparison of the numerical results was made for three different non-dimensional velocity components for a comprehensive discussion. In addition, detailed flow field analysis was conducted for both turbulence models. Within this, a safe helicopter approach pattern without any vortices and backflows can be determined. URANS and DES models were compared and a significant difference was observed in detailed flow field analysis. Finally, the numerical cases were extended to show the effects of the WOD angle for both turbulence models.

3.1 Numerical Uncertainty

The numerical approach in the present study involves two different turbulence models: unsteady RANS and DES. To show the uncertainty of the numerical method, the mesh algorithm used in the URANS approach was used for the verification study. A verification study for the DES mesh algorithm was not conducted since the mesh in the DES model is similar to the URANS model having higher mesh density over the flight deck. The verification study was carried out as recommended in the guidelines and procedures (Cosner et al., 2006; ITTC, 2014). The numerical approach was verified in terms of grid size since the time step size is already small enough. The numerical uncertainty was calculated using the GCI method based on Richardson extrapolation (1911) and proposed by Celik et al. (2008). Three different grid sizes were used to create fine, medium and coarse mesh. The details of the three-set GCI method can be found in recent studies in detail (Xing & Stern, 2010; Sezen et al., 2018, 2021; Dogrul, 2022). According to this method, the convergence condition (R) is calculated. The behavior of R shows the trend of convergence whether it has monotonic or oscillating convergence if $-1 < R < 1$. If the R value is out of this range, it means that the solution diverges (Xing & Stern, 2010).

Thus, the present study utilized, the fine, medium and coarse grid set and it is seen that the solution exhibited a monotonic convergence since $R < 1$ Roache (1998). The uncertainty value was calculated for the non-dimensional velocity magnitude derived from the components as a scalar function. The velocity components were obtained at 18 points for each grid number and the velocity magnitude was calculated, the numerical analysis condition is the headwind condition in which the flow comes to the ship with a heading angle of 0^0 with 10.3 m/s. For refining the grid number, the refinement factor was taken as $\sqrt{2}$. A brief mathematical definition of the verification method is given below.

$$R=\frac{\phi_{medium}-\phi_{fine}}{\phi_{coarse}-\phi_{medium}} \tag{15}$$

where R is the convergence condition while r is the refinement factor. In the three-set GCI method for the verification purpose, N_i stands for the grid number, $\emptyset_i$ represents the scalar function and U_N is the numerical uncertainty value as presented in Table 1.

As indicated in Table 1, the uncertainty values were presented for four different uncertainty methods given by (Xing & Stern, 2010). The uncertainty values are below

Table 1 Spatial uncertainty values for different verification methods

Parameter	U'_{mag}
N_{fine}	5615022
N_{medium}	2713346
N_{coarse}	1484526
$\emptyset_{fine}$	0.144756
$\emptyset_{medium}$	0.143058
$\emptyset_{coarse}$	0.140506
R	0.665
U_N (%) - GCI	1.638
U_N (%) - GCI1	1.142
U_N (%) - GCI2	2.741
U_N (%) - CF	2.104

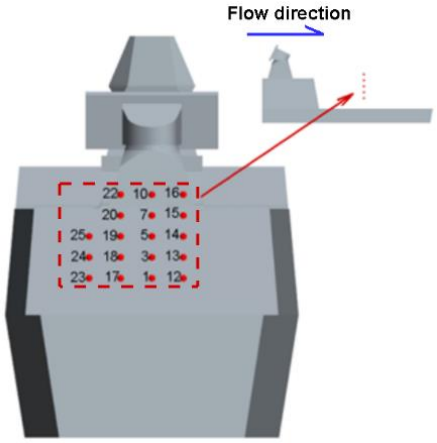

Fig. 7 Control points located over the fight deck

3% for all methods. It should be noted that the numerical method was verified in terms of the average value of velocity magnitude obtained from 18 points located over the flight deck.

3.2 Effect of Atmospheric Boundary Layer (ABL)

It is obvious that the airflow around a ship is affected heavily by the atmospheric processes and therefore it is imperative to consider the ABL in numerical studies to obtain accurate and reliable predictions on the airwake around the ship specifically over the flight deck. Several studies have been published in the literature on the flow around buildings (Abu-Zidan et al., 2020), terrain (Blocken et al., 2007) and SFS2 ship (Gnanamanickam et al., 2020) regarding the ABL. The effects of ABL on the airwake over the flight deck of NATO-GD ship were investigated by observing the velocity field at 18 different points located on the flight deck as done by (Owen et al., 2021). As shown in Fig. 7, these points were taken in transversal and vertical directions in the same streamwise direction.

The precise coordinates of these points are given in Table 2. The coordinates of the points are given for full-scale ship size. The x-coordinate of the points is kept as x=11.811 meters.

Table 2 Local coordinates of the control points according to ship bow

Control points	y (m)	z (m)	Control points	y (m)	z (m)
1	0	2.756	16	2.362	9.055
3	0	4.331	17	-2.362	2.756
5	0	5.906	18	-2.362	4.331
7	0	7.48	19	-2.362	5.906
10	0	9.055	20	-2.362	7.48
12	2.362	2.756	22	-2.362	9.055
13	2.362	4.331	23	-4.724	2.756
14	2.362	5.906	24	-4.724	4.331
15	2.362	7.48	25	-4.724	5.906

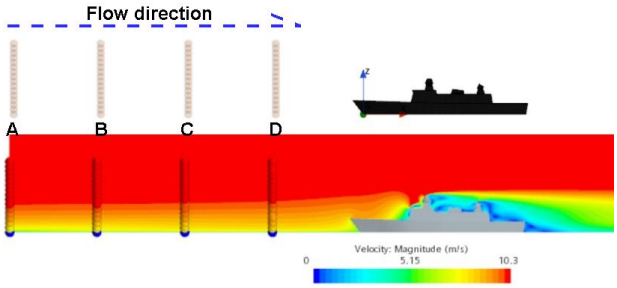

Fig. 8 ABL velocity profile at different planes coming to the ship

Three components of the velocity at the desired points were obtained for two different inflow conditions. The first scenario was based on the uniform velocity inlet condition where u=10.3 m/s. The second approach employs a user-defined field function to define the exact velocity field considering the ABL effects as described in the previous chapter. This section compares the experimental data provided by Owen et al. (2021) with the numerical results of the URANS approach without ABL effects as a comparison for the numerical technique concerning various velocity components computed at different flight deck locations.

Before the comparison of the numerical and experimental results, one should be sure that the desired velocity profile is defined to the flow inlet. For this purpose, the velocity values were obtained at four different planes upstream of the ship to show that the desired velocity profile could reach the ship superstructure precisely. The planes and the ship's location are shown in Fig. 8.

Figure 9 shows that the actual velocity profiles at different planes match well the desired velocity profile. This indicates that the atmospheric boundary layer was implemented in the numerical method with success.

Figure 10 shows the comparison of the numerical results of the URANS approach with the experimental data. The numerical findings include headwind condition with and without ABL profile Here, G0 stands for Green and zero angle which means the wind comes from the starboard side with zero angle. The following chapters show different angle results, namely G15 and G30 cases.

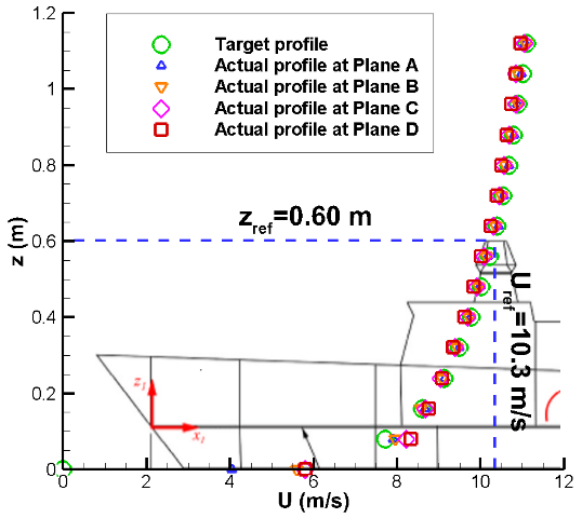

Fig. 9 Target and actual velocity profile obtained at different planes in the upstream of the ship

The results were compared with the experimental data (Owen et al., 2021) for three velocity components measured at 18 predefined points as given in Fig. 7. The velocity distributions show that the URANS results with the ABL profile match better with the experimental data for three velocity components. Especially for the x-component and z-component of the velocity, the ABL profile becomes important while it does not affect the y-component of the velocity. The relative difference is higher in the z-component while the trend is similar to the experiment. The results of the y-component agree quite well with the experiment, especially in the center points. From a general point of view, the results have higher discrepancy at the port and starboard side points while there is a good agreement at the center points.

3.3 Effect of Detached Eddy Simulation (DES) Modeling

For both URANS and DES models, Menter's Shear Stress Transport (SST) k-ω turbulence model (Menter, 1994, 2009) was utilized which is recommended for adverse pressure gradients and separating flows (Zhang, 2017) while the DES approach is also used for separated flows with reasonable computational cost regardless of Reynolds number (Travin et al., 2000; Zheng et al., 2016).

In addition to the results given in Fig. 10, Fig. 11 shows the numerical results of URANS and DES models compared with the experimental data for the ABL profile case. For the x-component of the velocity, at the points with the highest elevation (points 22, 10, 16), DES results show more discrepancy than the URANS results when compared with the experiments.

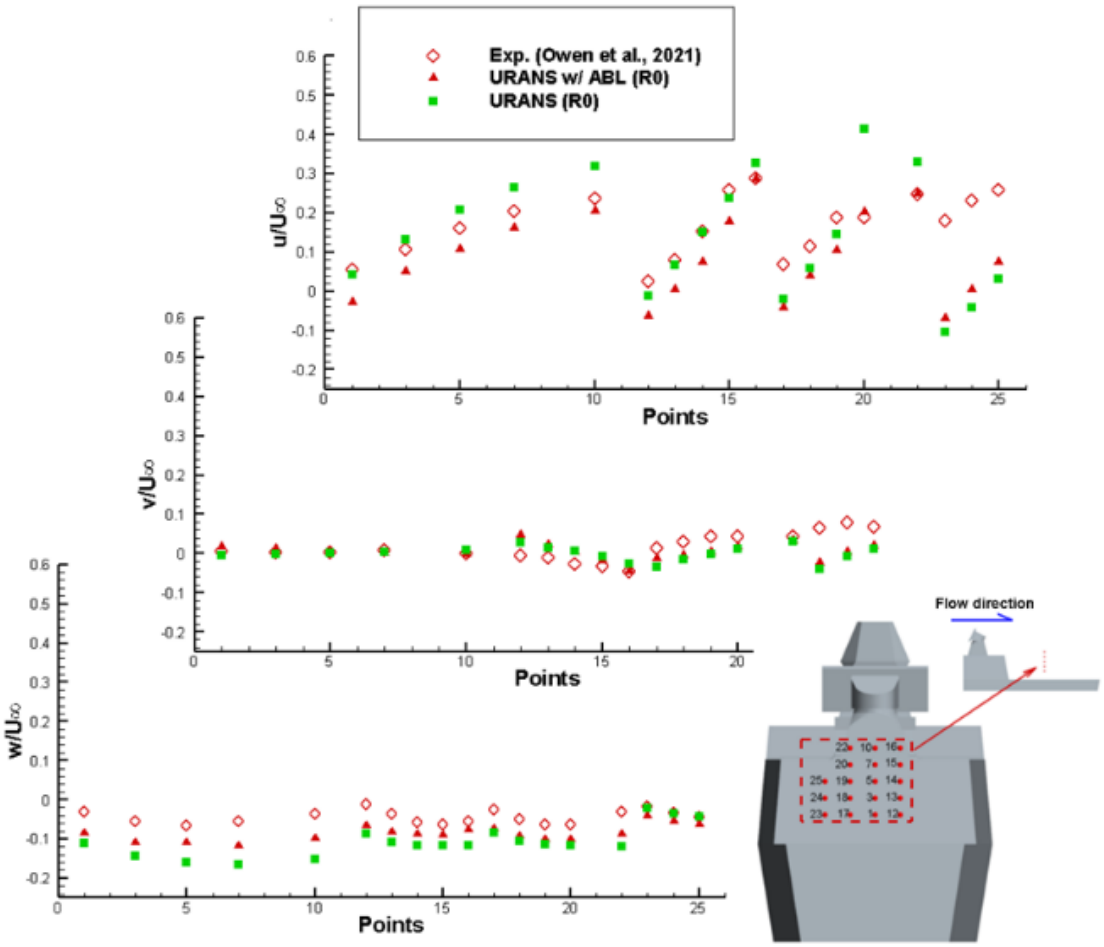

Fig. 10 Velocity distributions with and without ABL profile for URANS at WOD=0°

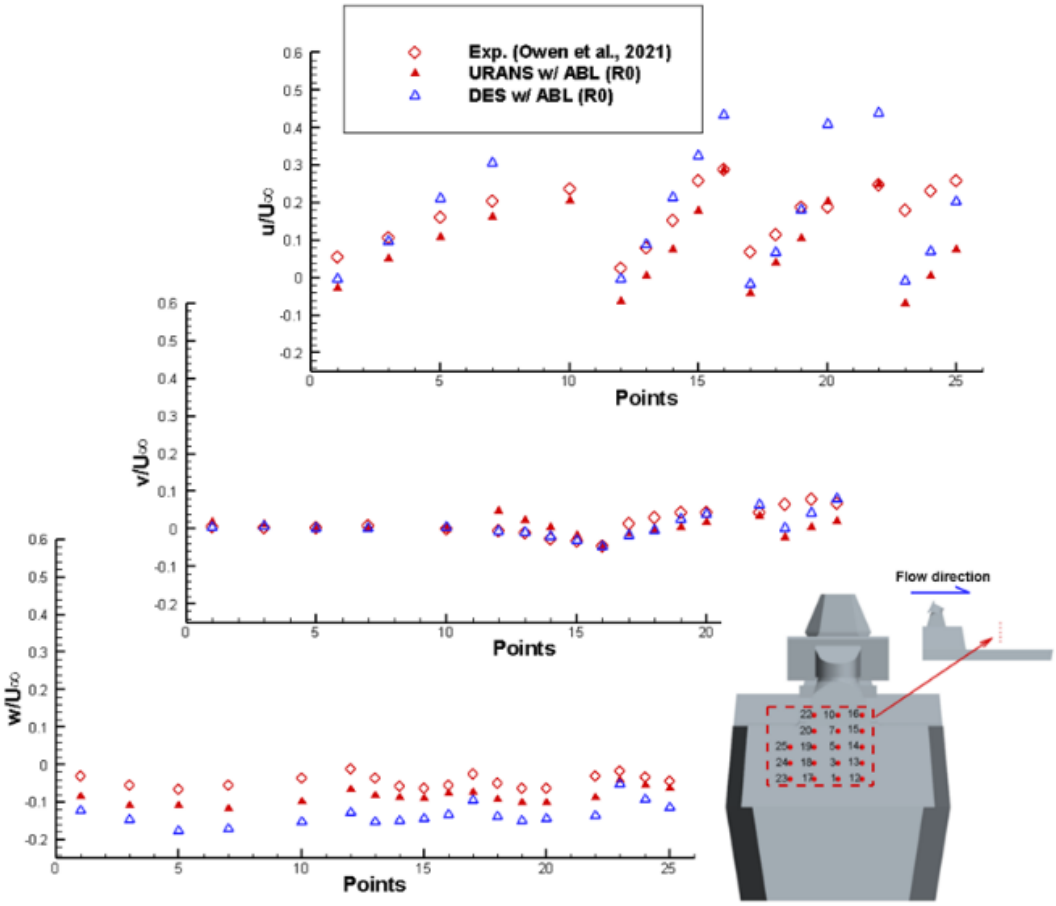

Fig. 11 Velocity distributions with ABL profile for URANS and DES at WOD=0°

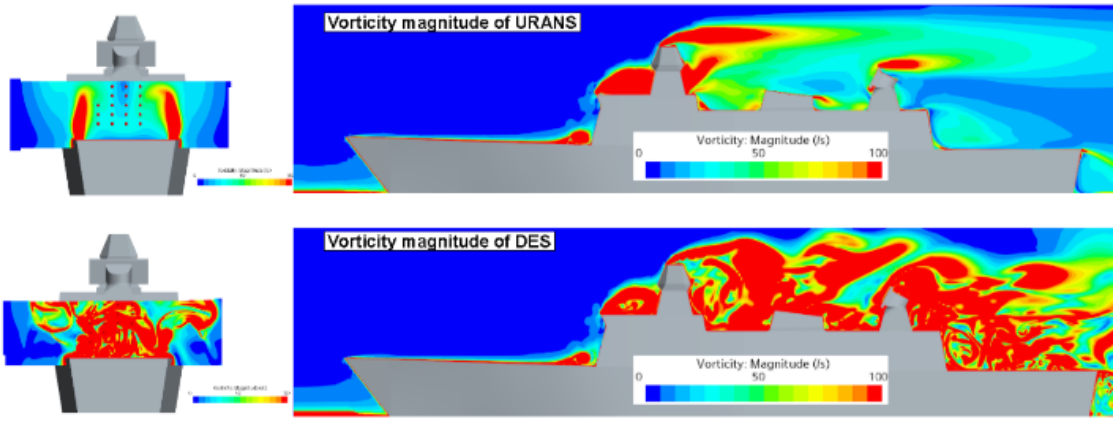

Fig. 12 Vorticity magnitude for URANS and DES at horizontal and transversal planes (WOD=0°)

At other points located in the centerline, port and starboard sides, both models have a good agreement while the DES model matches better with the experiments. The difference between experiments and the DES approach becomes smaller at the points located in the port and starboard sides when compared with the center points.

For the y-component of the velocity, at the points located in the centerline (points 1, 3, 5, 7, 10) URANS and DES results give similar results, however, at the points of port and starboard sides, the DES approach matches better. The z-component of the velocity shows a similar trend with the experiments for both URANS and DES models since URANS results match better. For the z-component, DES results show less difference at the outer located points on the port side (points 25, 24 and 23).

Figure 12 shows the difference between two turbulence models in terms of vorticity magnitude contours in two planes for headwind conditions (R0). As expected, the URANS approach provides minimal information about the vorticity field since the DES technique solves the whole vorticity field and displays the small eddies in the field. One may observe that the

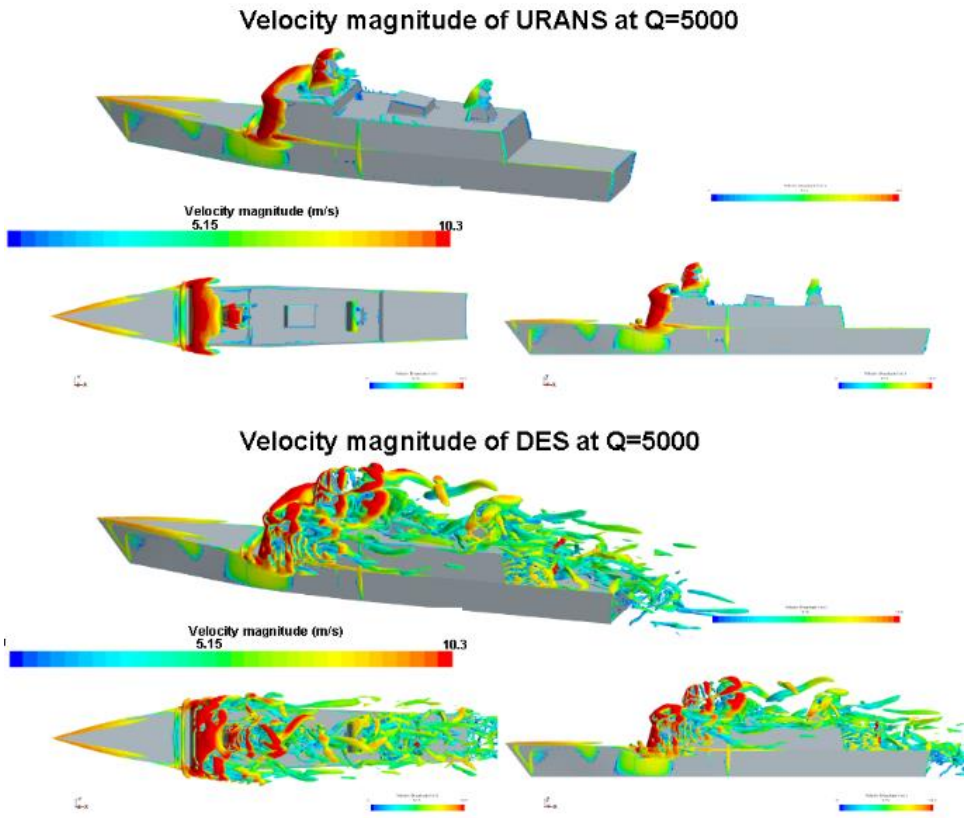

Fig. 13 Isosurfaces of Q-criterion colored with velocity magnitude for URANS and DES (WOD=0°)

reattachment region differs between URANS and DES models. URANS model predicts the same vorticity before the radar mast on the superstructure. After the mast geometry, the DES model predicts the vorticities with more detail.

Figure 13 shows the isosurfaces of Q-criterion colored with the velocity magnitude for both turbulence models for headwind conditions (R0). Q-criterion is widely used as a vortex identification method (Jeong & Hussain, 1995; Epps, 2017;) and there is no limitation for scalar quantity. For a fair comparison, the Q-criterion was chosen as Q=5000 in this study. Similar to Fig. 12, the vorticities cannot be seen behind the radar mast when the URANS simulation is employed while DES simulation can provide very detailed vortex structures over the ship superstructure.

Apart from the aforementioned 18 points used in the comparison of velocity components, detailed flow field analysis was carried out at six different planes located above the flight deck. Various parameters such as vorticity, helicity and turbulent kinetic energy were investigated to show the difference between URANS and DES models. Here, plane B is located in the middle of the hangar height while plane D is at the top of the hangar height. Planes E and F were located to visualize the wake downstream of the fire control radar (Fig. 14).

The comparison of the numerical methods in the present study was obtained for various velocity components at several points located in the middle of the flight deck. The results of the URANS and DES models

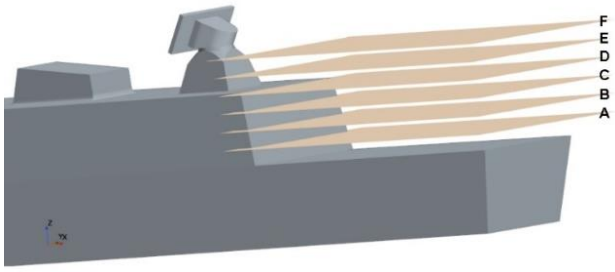

Fig. 14 Planes for flow-field analysis

are similar, however, even at some points DES model has more deviation from the experiments than the URANS model. For this reason, the velocity distribution at six plane sections was also given in Fig. 15 and 16 to illustrate the variance between URANS and DES models in analyzing the flow field details.

Figure 15 displays the URANS results showing the velocity magnitude at various elevations. As expected, inside the separation zone behind the superstructure, the velocity field is very low whereas on the sides there is little loss in velocity. In addition, one may observe the symmetry in the flow field in planes D to F, however, the radar is located upstream of these plane sections.

On the other hand, the DES results are much more helpful in discussing the flow field as given in Fig. 16. The flow is highly complex and asymmetrical at all elevations, as expected. The backflows coming inside the separation zone can be seen. There are some small vortices on the

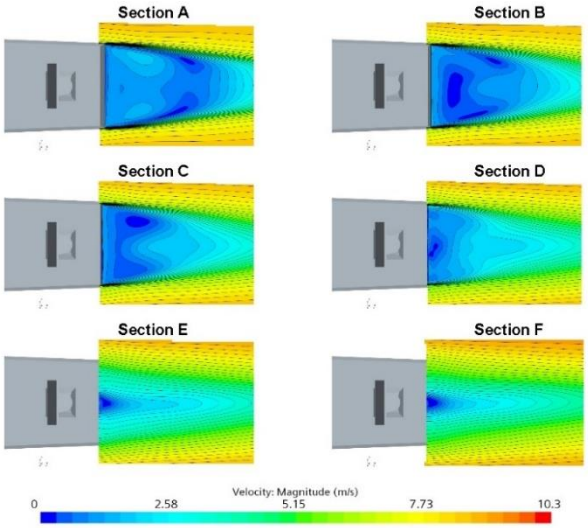

Fig. 15 Velocity distribution obtained with URANS model at various planes

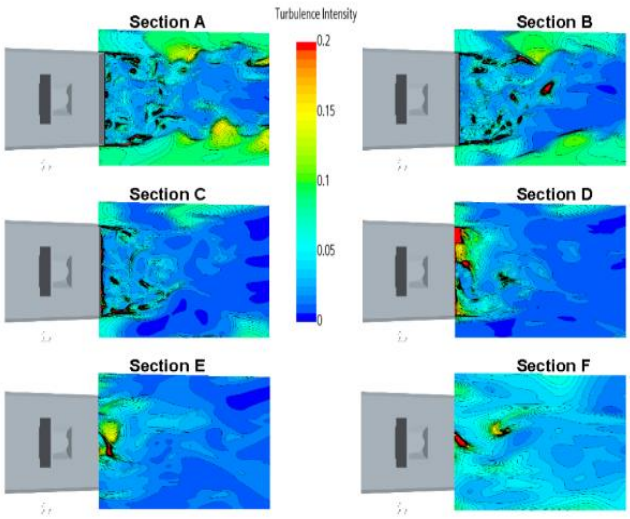

Fig. 17 Turbulence intensity obtained with DES model at various planes

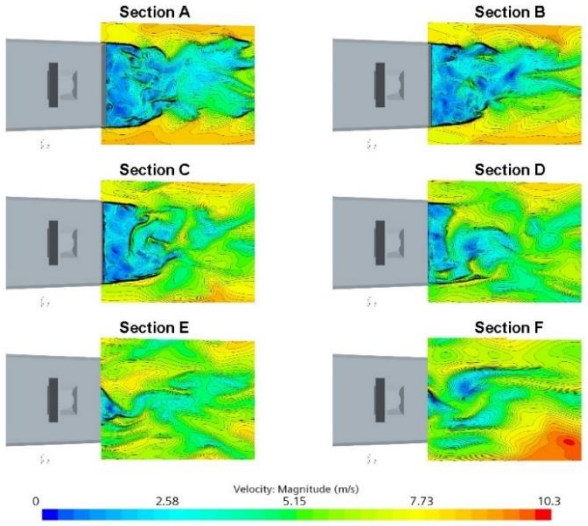

Fig. 16 Velocity distribution obtained with DES model at various planes

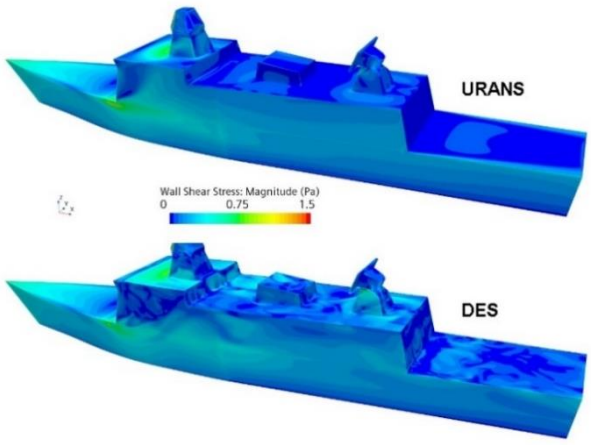

Fig. 18 Wall shear stress on the hull surface

sides because of the sharp edges of the hangar bay and the superstructure itself. The plane at the top which is located downstream of the fire control radar is strongly affected by this obstacle. The vortices vanish at the port side of the ship which may be a safe approach pattern for helicopters. At all elevations, this spot seems the safest zone for helicopters. Looking at Fig. 15 and 16, URANS poorly represents the rapid wind changes in the helicopter approach region, making the pattern appear safe for a helicopter operation. However, it can be concluded that the DES can highlight the challenging factors affecting flight safety in the specified areas.

In addition to the velocity distribution, turbulence intensity was calculated and given in contours in Fig. 17. Turbulence intensity is the ratio of the deviation in wind velocity to the true wind velocity. In many applications such as marine and offshore, turbulence intensity is limited to a constant value at different heights for safe helicopter operations. The turbulence intensity value should not exceed the limit or the helicopter operation may get into danger.

One may see from Fig. 17 that the lower elevations have complex and intense turbulence patterns due to their proximity to the flight deck and superstructure. The turbulence intensity decreases with the increase in the height from the deck and the vortex scales also become smaller. The elevation aligned with the radar is the safest pattern for safe helicopter operation.

Figure 18 depicts the wall shear stress on the hull surface obtained with both turbulence models.

The URANS results show that the wall shear stress is zero in almost all locations on the flight deck which means there is nearly no flow separation on the deck surface. On the other side, the DES results highlight the flow separations on the flight deck more realistically. One may observe that both the URANS and DES models yield almost similar velocity components at the specified points over the flight deck, however, the DES model more accurately predicts the flow separations on the deck surface. Again, the URANS method indicates no deck

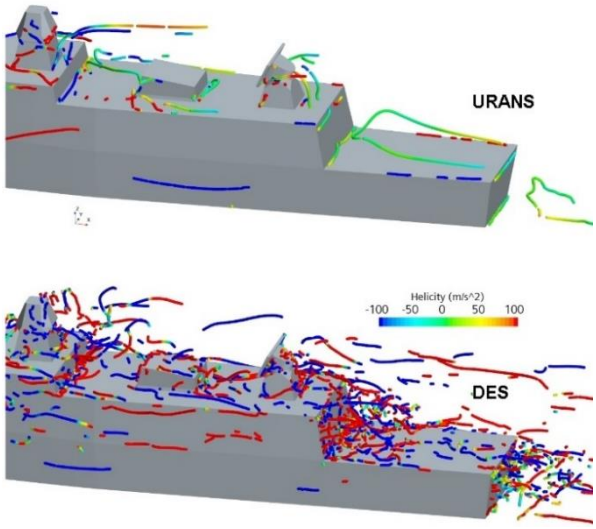

Fig. 19 Vortex cores around the superstructure colored by helicity

surface separation while DES shows the flow separation posing danger to flight personnel on the flight deck.

Figure 19 shows the vortex cores indicating the center of the vortices around the superstructure colored by helicity. Attention given to the region behind the hangar bay makes it clear that there are complex vortex cores in opposite directions since the blue and red colors indicate the negative and positive values of helicity determining the direction of the vortices. The URANS model only shows a helical vortex core above the flight deck while the DES model simulates smaller helical vortex cores having different directions. It can be seen that the vortex cores vanish after half of the flight deck in the axial direction.

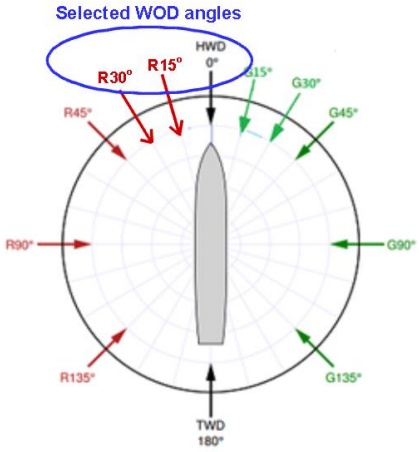

Fig. 20 Relative wind angles highlighting the selected cases (WOD=0°, 15° and 30°) in the study

3.4 Effect of Wind-Over-Deck (WOD) Angle

Helicopter operations over a naval surface combatant's flight deck are conducted not at all wind angles. Mostly, bow quartering scenarios are particularly significant during landing and take-off operations, for this reason, wind over deck angles of 0, 15 and 30 degrees as given in Fig. 20 were taken into consideration. In Fig. 20, HWD and TWD stand for Headwind Direction and Tailwind Direction, respectively. R15 and R30 mean that the wind is coming from the port side (Red).

Figure 21 shows the results of the URANS approach for three different wind-over-deck angles of 0, 15 and 30 degrees. For the x-component of the velocity, at all points, the headwind with zero angle mostly diverts from form bow-quartering wind angles. Considering the wind comes from the port side as shown in Fig. 21, at the points on the

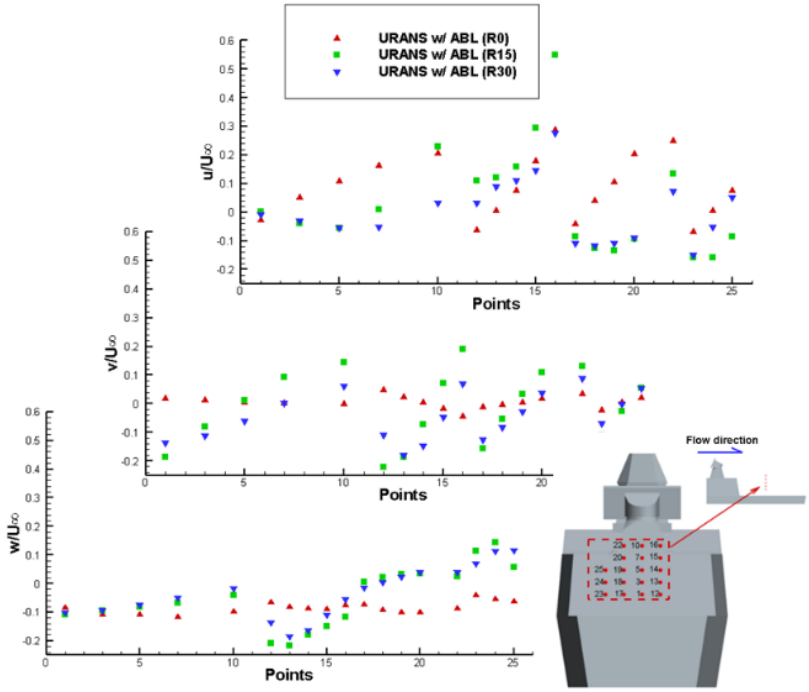

Fig. 21 Velocity distributions with ABL profile for URANS at WOD=0°, 15° and 30°

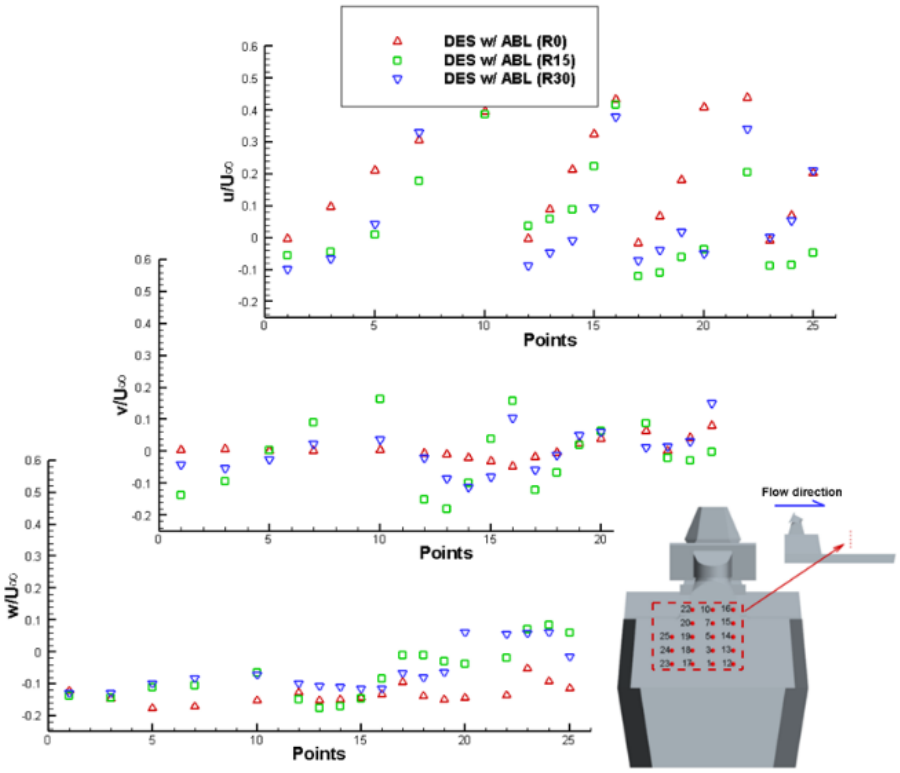

Fig. 22 Velocity distributions with ABL profile for DES at WOD=0°, 15° and 30°

starboard side (points 12, 13, 14, 15, 16), the relative wind angle has some effects on the velocity distribution while at the points in the port side (points 17, 18, 19, 20, 22), there is nearly no effect for 15 and 30 degrees.

For the y-component of the velocity, again the zero angle (headwind) results divert from other relative wind angles. There are some discrepancies between 15 and 30 degrees at all points while the velocity distribution trends of both angles are similar. At the outer port side (points 23, 24, 25), there is nearly no WOD angle effect on the velocity distribution.

For the z-component of the velocity, very little angle effect is observed at the centerline points. However, at the starboard and port sides, the findings for the headwind diverge from other results and the distribution is almost the same at 15 and 30 degrees of relative wind angle.

The outcomes of the DES technique are displayed in Fig. 22 for three different wind-over-deck angles of 0, 15 and 30 degrees. For the x-component of the velocity, at all points, the headwind angle separates from other wind angles while there is minimal difference between 15 and 30 degrees at the centerline points. As seen in Fig. 15, the flow behavior obtained with DES and URANS approaches is generally comparable.

Figure 23 shows the velocity distribution at different elevations behind the superstructure obtained by URANS for R15 wind condition which means the wind comes from the port side with an angle of 15 degrees. For this wind case, the wind sweeps the flow at the port side, as expected. However, at almost all elevations, the effect of the wind direction is limited up to the hangar height. In the downstream region of the fire control radar, the flow is more affected.

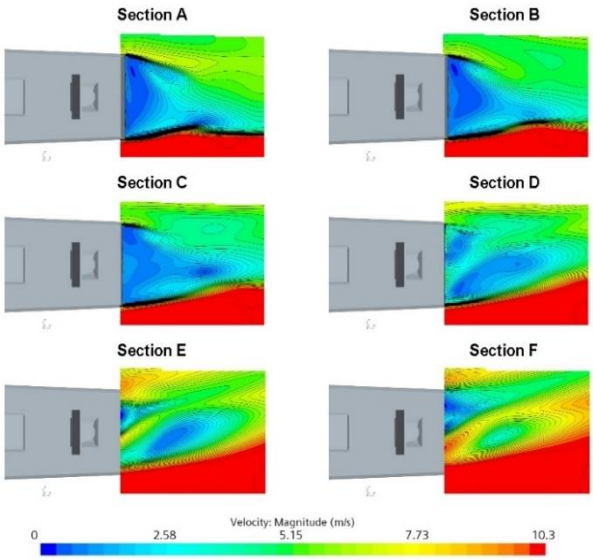

Fig. 23 Velocity distribution obtained with URANS model for R15 wind condition

Figure 24 shows the results of the DES model shows the effect of the wind direction more clearly. Apart from the URANS model, a significant change in the backflow regions can be observed. Behind the hangar bay, the separation zone nearly stands while backflows occur downstream of the radar with the change in the wind angle when compared with the headwind condition (R0). Similar to the headwind condition, the URANS model fails to show the detailed flow structures when compared with the DES model. Especially in Fig. 24, backflows and wind changes over the hangar bay are observed which may give an idea for a safe approach pattern for the helicopters.

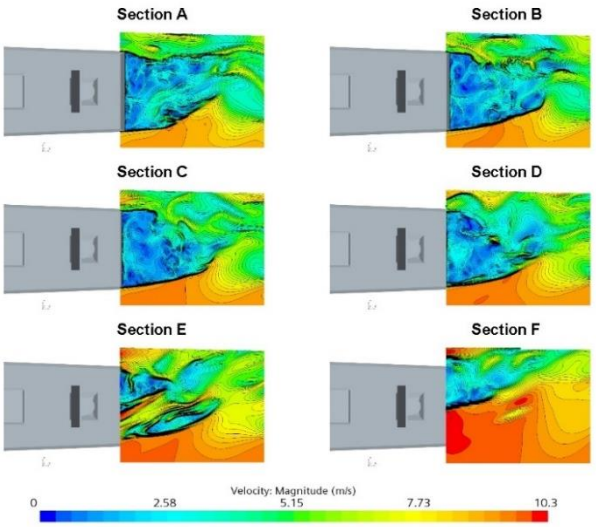

Fig. 24 Velocity distribution obtained with DES model for R15 wind condition

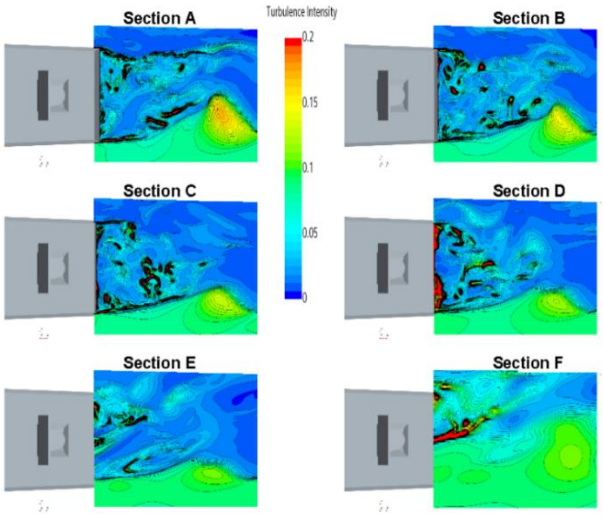

Fig. 25 Turbulence intensity obtained with DES model for R15 wind condition

Figure 25 shows the turbulence intensity over the flight deck at various elevations for R15 wind condition. When compared with the headwind (R0) condition, the complexity of the flow and turbulence intensity increases significantly. However, a safer zone occurs on the starboard side even at low heights since the wind is coming from the port side.

Regarding the wall shear stress, as shown in Fig. 26, the flow separation on the flight deck surface becomes more visible in the DES model while the URANS model still shows little separation similar to the headwind condition.

Figure 27 and 28 show the velocity distribution at different elevations behind the superstructure for the wind-over-deck (WOD) angle of 30 degrees. In this case, the wind is considered as coming from the port side, the wind direction effects are more clear at the upper heights. The pilot should be aware of a large vortex that forms on

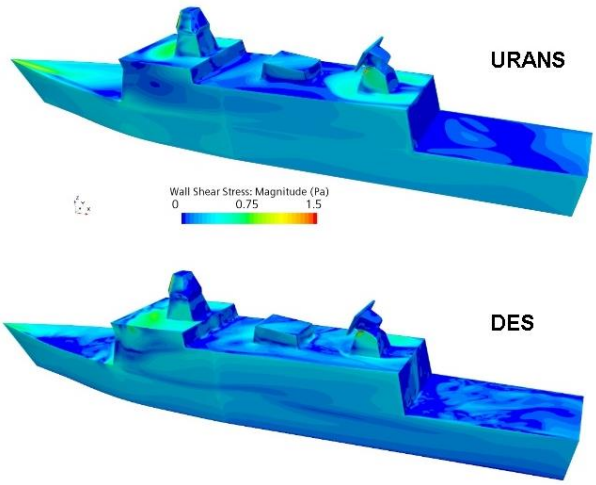

Fig. 26 Wall shear stress on the hull surface for R15 wind condition

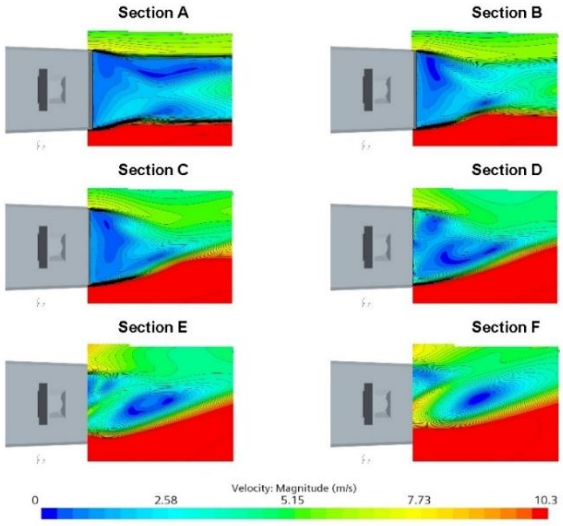

Fig. 27 Velocity distribution obtained with URANS model for R30 wind condition

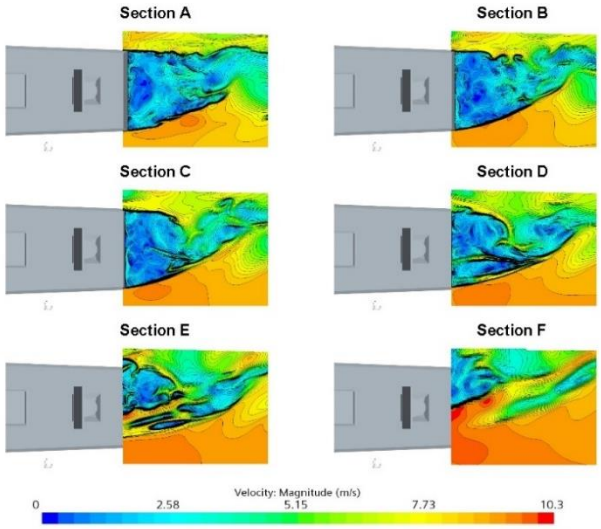

Fig. 28 Velocity distribution obtained with DES model for R30 wind condition

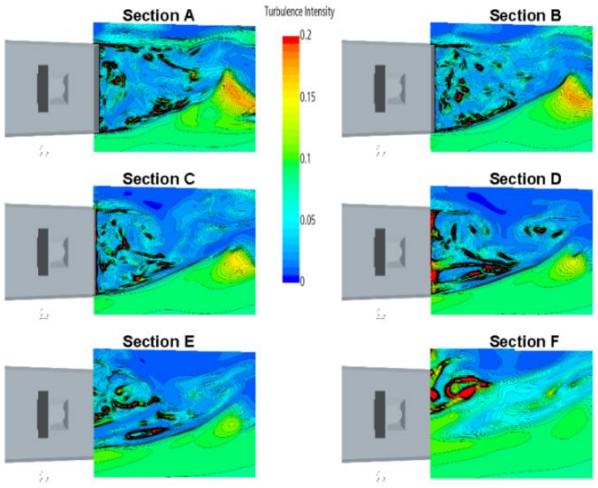

Fig. 29 Turbulence intensity obtained with DES model for R30 wind condition

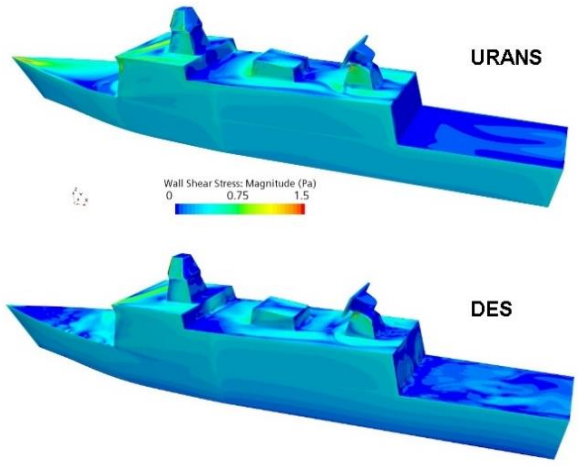

Fig. 30 Wall shear stress on the hull surface for R30 wind condition

the plane downstream during the helicopter operation. The DES results, inherently, simulate this flow field with more detail. The wind angle effects become more visible behind the radar because the superstructure itself blocks the vortices at lower heights which are located behind the hangar bay. The flow field behind the radar is strongly affected by the wind direction, the vortices become bigger and flow separations break into small separation zones that might be dangerous for safe helicopter operations.

Figure 29 shows the turbulence intensity over the flight deck at various elevations for R30 wind condition. In this condition, the wind angle effect becomes clear at all elevations. The safer operation zone compared with R0 condition becomes smaller in this condition.

This means that the wind angle affects the airwake significantly and there is not a linear relation between angle and low turbulence regions. R15 wind creates a low turbulence region on the starboard side while R30 wind breaks it at all elevations.

Figure 30 shows the wall shear stress on the flight deck surface for R30 wind condition. URANS model underestimates the flow separations on the surface, while the DES model provides more information in detail regarding the flow separation.

4. CONCLUSION

In this study, the numerical investigation of ship airwake around NATO-GD was carried out using two different mesh structures and turbulence models employing URANS and DES methods. The numerical setup was verified in terms of grid size for URANS using four different uncertainty methods and the average uncertainty value was found less than 2%. Following this, the numerical analyses were extended by utilizing an ABL velocity profile and DES model, respectively. The results were compared with the experimental data available in open literature and a fair comparison was made for three different velocity components over the flight deck. In particular, x- and y-components have better agreement with the experiments. Additionally, the results demonstrated that the ABL utilized yields promising results. This is because the wind tunnel experiments selected for comparisons have already a default non-uniform velocity profile.

DES turbulence model was used with denser mesh structure and the results have a good agreement with the experiments and URANS model. However, at the points located on the sides of the flight deck where the vortices occur, the DES results have better agreement than the URANS results. Finally, three WOD angles were investigated for both turbulence models with ABL profile. Particularly for the detailed flow analysis, the DES model is more reliable in terms of the local velocity field. In addition to the comparison points, planes were located at different elevations over the flight deck and velocity distributions were obtained at these surfaces. DES model showed details of the flow separations, backflows and vortex structures on the flow field while the URANS model was insufficient. There were almost no vortices or separations in the flight region and on the flight deck surface according to the URANS data that might result in an inaccurate assessment of the helicopter operations. However, DES results showed many details of the flow field over the flight deck. The flow separations and sudden changes in the velocity field were easily modeled using the DES model. The flow field data obtained with the DES model is very significant for safe helicopter operations. In conclusion, URANS and DES models were in good agreement with the experimental data at the specified points in terms of velocity components. On the other hand, if it is aimed to observe the details of the flow field precisely, it is vital to use the DES model in the numerical analyses. DES model enables to obtain vortex structures in small and large scales, stagnation points at different heights. This would be useful to determine safe helicopter operation patterns.

In further studies, the helicopter rotor can be included in the study to investigate the ship-rotor interaction numerically. In addition, free surface effects and ship motions can be integrated into the flow physics.

ACKNOWLEDGEMENTS

This study was supported by Scientific and Technological Research Council of Türkiye (TÜBİTAK) ARDEB 1002 - Short Term R&D Funding Program, Grant No 222M375.

CONFLICT OF INTEREST

The authors declare that they have no known competing financial interests or personal relationships that could have appeared to influence the work reported in this paper.

AUTHORS CONTRIBUTION

Sarih Sarı: Formal analysis, Investigation, Methodology, Writing – original draft, Writing – review & editing. **Ali Doğrul:** Conceptualization, Formal analysis, Methodology, Resources, Writing – review & editing. **Seyfettin Bayraktar:** Conceptualization, Funding acquisition, Project administration, Resources, Writing – review & editing.

REFERENCES

Abu-Zidan, Y., Mendis, P., & Gunawardena, T. (2020). Impact of atmospheric boundary layer inhomogeneity in CFD simulations of tall buildings. *Heliyon*, *6*(7), e04274. https://doi.org/10.1016/j.heliyon.2020.e04274

Cindori, M., Čajić, P., Džijan, I., Juretić, F., & Kozmar, H. (2022). A comparison of major steady RANS approaches to engineering ABL simulations. *Journal of Wind Engineering and Industrial Aerodynamics*, 221, 104867. https://doi.org/10.1016/j.jweia.2021.104867

Bardera, R.; Matias, J. C.; García-Magariño, A. Experimental validation of aerodynamic computational results in the aft-deck of a simplified frigate shape (SFS2). A: MARINE VIII. MARINE VIII: *proceedings of the VIII International Conference on Computational Methods in Marine Engineering*. CIMNE, 2019, p. 405-416. ISBN 978-84-949194-3-5

Blocken, B., Stathopoulos, T., & Carmeliet, J. (2007). CFD simulation of the atmospheric boundary layer: Wall function problems. *Atmospheric Environment*, *41*(2), 238–252. https://doi.org/10.1016/j.atmosenv.2006.08.019

Bogstad, M. C., Habashi, W. G., Akel, I., Ait-Ali-Yahia, D., Giannias, N., & Longo, V. (2002). Computational-fluid-dynamics based advanced ship-airwake database for helicopter flight simulators. *Journal of Aircraft*, *39*(5), 830–838. https://doi.org/10.2514/2.3003

Celik, I. B., Ghia, U., Roache, P. J., Freitas, C. J., & Raad, P. E. (2008). Procedure for estimation and reporting of uncertainty due to discretization in CFD applications. *Journal of Fluids Engineering*, *130*(7). https://doi.org/10.1115/1.2960953

Cook, N. J. (1997). The Deaves and Harris ABL model applied to heterogeneous terrain. *Journal of Wind Engineering and Industrial Aerodynamics*, *66*(3), 197–214. https://doi.org/10.1016/S0167-6105(97)00034-2

Cosner, R., Oberkampf, B., Rumsey, C., Rahaim, C., & Shih, T. (2006). *AIAA committee on standards for computational fluid dynamics: status and plans*. 44th AIAA Aerospace Sciences Meeting and Exhibit. American Institute of Aeronautics and Astronautics. https://doi.org/10.2514/6.2006-889

Dogrul, A. (2022). Numerical prediction of scale effects on the propulsion performance of JOUBERT BB2 submarine. *Brodogradnja : Teorija i Praksa Brodogradnje i Pomorske Tehnike*, *73*(2), 17–42. https://doi.org/10.21278/brod73202

Dooley, G. M., Krebill, A. F., Martin, J. E., Buchholz, J. H. J., & Carrica, P. M. (2020a). Structure of a Ship Airwake at Multiple Scales. *AIAA Journal*, *58*(5), 2005–2013. https://doi.org/10.2514/1.J058994

Dooley, G., Ezequiel Martin, J., Buchholz, J. H. J., & Carrica, P. M. (2020b). Ship airwakes in waves and motions and effects on helicopter operation. *Computers & Fluids*, *208*, 104627. https://doi.org/10.1016/j.compfluid.2020.104627

Epps, B. (2017, January 9). *Review of vortex identification methods.* 55th AIAA Aerospace Sciences Meeting. https://doi.org/10.2514/6.2017-0989

Forrest, J. S., & Owen, I. (2010). An investigation of ship airwakes using detached-eddy simulation. *Computers & Fluids*, *39*(4), 656–673. https://doi.org/10.1016/j.compfluid.2009.11.002

Gnanamanickam, E. P., Zhang, Z., Seth, D., & Leishman, J. G. (2020, June 15). *Structure of the ship airwake in a simulated atmospheric boundary layer*. AIAA Aviation 2020 Forum. Aiaa Aviation 2020 Forum, Virtual Event. https://doi.org/10.2514/6.2020-2702

Gritskevich, M. S., Garbaruk, A. V., Schütze, J., & Menter, F. R. (2012). Development of DDES and IDDES formulations for the k-ω shear stress transport model. *Flow, Turbulence and Combustion*, *88*(3), 431–449. https://doi.org/10.1007/s10494-011-9378-4

ITTC. (2014). *7.5-03-01-01 uncertainty analysis in CFD, verification and validation methodology and procedures.* ITTC - Recommended Procedures and Guidelines.

Jeong, J., & Hussain, F. (1995). On the identification of a vortex. *Journal of Fluid Mechanics*, *285*, 69–94. https://doi.org/10.1017/S0022112095000462

Li, T., Wang, Y. B., Zhao, N., & Qin, N. (2020). An investigation of ship airwake over the frigate afterbody. *International Journal of Modern Physics B*, *34*(14n16), 2040069. https://doi.org/10.1142/S021797922040069X

Major, D., Schmitz, S., Shipman, J. D., Bin, J., & Polsky, S. (2023, June 12). *Assessment of numerical methods for ship airwake simulations with unsteady atmospheric boundary-layer effects*. AIAA AVIATION 2023 Forum. AIAA AVIATION 2023 Forum, San Diego, CA and Online. https://doi.org/10.2514/6.2023-3692

Menter, F. R. (1994). Two-equation eddy-viscosity turbulence models for engineering applications. *AIAA Journal*, *32*(8), 1598–1605. https://doi.org/10.2514/3.12149

Menter, F. R. (2009). Review of the shear-stress transport turbulence model experience from an industrial perspective. *International Journal of Computational Fluid Dynamics*, *23*(4), 305–316. https://doi.org/10.1080/10618560902773387

Nisham, A., Terziev, M., Tezdogan, T., Beard, T., & Incecik, A. (2021). Prediction of the aerodynamic behaviour of a full-scale naval ship in head waves using Detached Eddy Simulation. *Ocean Engineering*, *222*, 108583. https://doi.org/10.1016/j.oceaneng.2021.108583

Owen, I., Lee, R., Wall, A., & Fernandez, N. (2021). The NATO generic destroyer – a shared geometry for collaborative research into modelling and simulation of shipboard helicopter launch and recovery. *Ocean Engineering*, *228*, 108428. https://doi.org/10.1016/j.oceaneng.2020.108428

Owen, I., Scott, P., & White, M. (2014). The effect of ship size on the flying qualities of maritime helicopters. *In the American Helicopter Society 70th Annual Forum*, Montreal, Quebec, Canada.

Reddy, K. R., Toffoletto, R., & Jones, K. R. W. (2000). Numerical simulation of ship airwake. *Computers & Fluids*, *29*(4), 451–465. https://doi.org/10.1016/S0045-7930(99)00033-X

Ren, X., Su, H., Yu, H. H., & Yan, Z. (2022). Wall-modeled large eddy simulation and detached eddy simulation of wall-mounted separated flow via OpenFOAM. *Aerospace*, *9*(12), 12. https://doi.org/10.3390/aerospace9120759

Richards, P. J., & Hoxey, R. P. (1993). Appropriate boundary conditions for computational wind engineering models using the k-ϵ turbulence model. *Journal of Wind Engineering and Industrial Aerodynamics*, *46–47*, 145–153. https://doi.org/10.1016/0167-6105(93)90124-7

Richardson, L. F. (1911). The approximate arithmetical solution by finite differences of physical problems involving differential equations, with an application to the stresses in a masonry dam. *Philosophical Transactions of the Royal Society of London. Series A, Containing Papers of a Mathematical or Physical Character*, *210*, 307–357.

Roache, P. J. (1998). Verification of codes and calculations. *AIAA Journal*, *36*(5), 696–702. https://doi.org/10.2514/2.457

Rosenfeld, N., Kimmel, K., & Sydney, A. J. (2015, January 5). *Investigation of ship topside modeling practices for wind tunnel experiments. 53rd AIAA Aerospace Sciences Meeting.* 53rd AIAA Aerospace Sciences Meeting, Kissimmee, Florida. https://doi.org/10.2514/6.2015-0245

Sarı, S., Dogrul, A., & Bayraktar, S. (2022). *The aerodynamic wind loads of a naval surface combatant in model scale.* New Technologies, Development and Application V, Isak Karabegović, Ahmed Kovačević, Sadko Mandžuka, Editor, Springer Nature.

Seth, D., Zhang, Z., Gnanamanickam, E. P., & Leishman, J. G. (2020, June 15). Time-resolved PIV measurements of a ship airwake in a simulated atmospheric boundary layer. *AIAA Aviation 2020 Forum*. AIAA Aviation 2020 Forum, Virtual Event. https://doi.org/10.2514/6.2020-2701

Setiawan, H., Kevin, Philip, J., & Monty, J. P. (2022). Turbulence characteristics of the ship air-wake with two different topside arrangements and inflow conditions. *Ocean Engineering*, *260*, 111931. https://doi.org/10.1016/j.oceaneng.2022.111931

Sezen, S., Delen, C., Dogrul, A., & Atlar, M. (2021). An investigation of scale effects on the self-propulsion characteristics of a submarine. *Applied Ocean Research*, *113*, 102728. https://doi.org/10.1016/j.apor.2021.102728

Sezen, S., Dogrul, A., Delen, C., & Bal, S. (2018). Investigation of self-propulsion of DARPA Suboff by RANS method. *Ocean Engineering*, *150*, 258–271. https://doi.org/10.1016/j.oceaneng.2017.12.051

Shi, Y., Li, G., Su, D., & Xu, G. (2020). Numerical investigation on the ship/multi-helicopter dynamic interface. *Aerospace Science and Technology*, *106*, 106175. https://doi.org/10.1016/j.ast.2020.106175

Shipman, J. D., & Bin, J. (2021.). *Atmospheric boundary layer turbulence simulation for ship airwake CFD applications.* AIAA Aviation 2021 Forum. american institute of aeronautics and astronautics. https://doi.org/10.2514/6.2021-2481

Shukla, S., Singh, S. N., Sinha, S. S., & Vijayakumar, R. (2021). Comparative assessment of URANS, SAS and DES turbulence modeling in the predictions of massively separated ship airwake characteristics. *Ocean Engineering*, *229*, 108954. https://doi.org/10.1016/j.oceaneng.2021.108954

Spalart, P. R. (2001). *Young-person's guide to detached-eddy simulation grids* (NASA/CR-2001-211032).

Su, D., Xu, G., Huang, S., & Shi, Y. (2019). Numerical investigation of rotor loads of a shipborne coaxial-rotor helicopter during a vertical landing based on moving overset mesh method. *Engineering Applications of Computational Fluid Mechanics*, *13*(1), 309–326. https://doi.org/10.1080/19942060.2019.1585390

Taymourtash, N., Zanotti, A., Gibertini, G., & Quaranta, G. (2022). Unsteady load assessment of a scaled-

helicopter model in a ship airwake. *Aerospace Science and Technology*, 107583. https://doi.org/10.1016/j.ast.2022.107583

Thornhill, E., Wall, A., McTavish, S., & Lee, R. (2020). Ship anemometer bias management. *Ocean Engineering*, *216*, 107843. https://doi.org/10.1016/j.oceaneng.2020.107843

Travin, A., Shur, M., Strelets, M., & Spalart, P. (2000). Detached-eddy simulations past a circular cylinder. *Flow, Turbulence and Combustion*, *63*(1), 293–313. https://doi.org/10.1023/A:1009901401183

Wall, A., Thornhill, E., Barber, H., McTavish, S., & Lee, R. (2022). Experimental investigations into the effect of at-sea conditions on ship airwake characteristics. *Journal of Wind Engineering and Industrial Aerodynamics*, *223*, 104933. https://doi.org/10.1016/j.jweia.2022.104933

Watson, N. A., White, M., & Owen, I. (2019, June 17). *Experimental validation of the unsteady CFD-generated airwake of the HMS queen elizabeth aircraft carrier*. AIAA Aviation 2019 Forum. AIAA Aviation 2019 Forum, Dallas, Texas, USA. https://doi.org/10.2514/6.2019-3029

Wilcox, D. C. (2006). *Turbulence modeling for CFD* (3rd edition). DCW Industries.

Wilcox, D. C. (2008). Formulation of the k-w turbulence model revisited. *AIAA Journal*, *46*(11), 2823–2838. https://doi.org/10.2514/1.36541

Xing, T., & Stern, F. (2010). Factors of safety for richardson extrapolation. *Journal of Fluids Engineering*, *132*(6). https://doi.org/10.1115/1.4001771

Yuan, W., Lee, R., & Wall, A. (2016, September 23). *Combined numerical and experimental simulations of unsteady ship airwakes*. 30th Congress of the International Council of the Aeronautical Sciences, Daejeon, Korea.

Yuan, W., Wall, A., & Lee, R. (2018). Combined numerical and experimental simulations of unsteady ship airwakes. *Computers & Fluids*, *172*, 29–53. https://doi.org/10.1016/j.compfluid.2018.06.006

Zamiri, A., & Chung, J. T. (2023). Numerical evaluation of wind direction effects on the turbulence aerodynamics of a ship airwake. *Ocean Engineering*, *284*, 115104. https://doi.org/10.1016/j.oceaneng.2023.115104

Zhang, D. (2017). Comparison of various turbulence models for unsteady flow around a finite circular cylinder at Re=20000. *Journal of Physics: Conference Series*, *910*(1), 012027. https://doi.org/10.1088/1742-6596/910/1/012027

Zheng, W., Yan, C., Liu, H., & Luo, D. (2016). Comparative assessment of SAS and DES turbulence modeling for massively separated flows. *Acta Mechanica Sinica*, *32*(1), 12–21. https://doi.org/10.1007/s10409-015-0505-7

Zhu, N., Zhang, Z., Gnanamanickam, E., & Gordon Leishman, J. (2023, January 23). *Effects of a Simulated Atmospheric Boundary Layer on Ship Airwakes*. AIAA Scitech 2023 Forum. https://doi.org/10.2514/6.2023-0470

Zhu, N., Zhang, Z., Gnanamanickam, E., & Leishman, J. G. (2022, January 3). *Dynamics of large-scale flow structures within ship airwakes*. AIAA Scitech 2022 Forum. https://doi.org/10.2514/6.2022-2532